ADVANCED FUNCTIONAL MATERIALS
www.afm-journal.de

Ultrathin Graphene Nanofiltration Membrane for Water Purification

*Yi Han, Zhen Xu, and Chao Gao**

A method of fabricating ultrathin (≈22–53 nm thick) graphene nanofiltration membranes (uGNMs) on microporous substrates is presented for efficient water purification using chemically converted graphene (CCG). The prepared uGNMs show well packed layer structure formed by CCG sheets, as characterized by scanning electron microscopy, atomic force microscopy, and transmission electron microscopy. The performance of the uGNMs for water treatment was evaluated on a dead end filtration device and the pure water flux of uGNMs was high (21.8 L m^{-2} h^{-1} bar^{-1}). The uGNMs show high retention (>99%) for organic dyes and moderate retention (≈20–60%) for ion salts. The rejection mechanism of this kind of negatively charged membranes is intensively studied, and the results reveal that physical sieving and electrostatic interaction dominate the rejection process. Because of the ultrathin nature of uGNMs, 34 mg of CCG is sufficient for making a square meter of nanofiltration membrane, indicating that this new generation graphene-based nanofiltration technology would be resource saving and cost-effective. The integration of high performance, low cost, and simple solution-based fabrication process promises uGNMs great potential application in practical water purification.

1. Introduction

In the coming decade, the lack of clean water is a formidable challenge because of rapid population growth, extended droughts and fast growing demands. Among all the possible solutions for the water resources crisis, low cost and high efficient nanofiltration might be the most promising one. Nanofiltration technology is now widely used in drinking water and waste water treatments due to its low energy cost and simple operational process, in which the properties of nanofiltration membranes (NFMs) are of vital importance.[1–3] Generally, most of polymeric NFMs have advantages of flexibility, simple preparation process, and relatively low cost, but also face some problems, such as poor chemical resistance, limited lifetime, and membrane fouling.[4] On the contrary, inorganic ceramic NFMs possess the merits of thermal stability, certain solvent resistance, high strength, and long lifetime, whereas have drawbacks of complex fabrication process, high cost, and brittleness.[5] Hence, an ideal NFM would be made by a polymeric NFM-like solution-based simple process, and simultaneously combine the fine attributes of both membranes. However, to access such a NFM is still a big challenge unresolved hitherto.[6,7]

The emergence of carbon nanotubes (CNTs) casts a light on achieving the ideal NFMs, since CNTs not only possess the ceramic-like stability, but also the polymer-like flexibility and possible processibility.[8] Moreover, CNTs could provide unique 1D nanochannel for water transporting. Intensively theoretical calculations predicted that the permeation of water through a CNT is extremely fast.[9–13] Hinds and co-workers experimentally investigated mass transport through aligned multiwalled CNT membranes with pore diameter around 7 nm, and, indeed, reported their high water flux, over 4 orders of magnitude larger than conventional hydrodynamic flow prediction.[14] Several reports have also explored the use of vertically-aligned CNTs membranes for filtration and separation applications.[15–20] Undoubtedly, aligned CNTs membranes are a fine model for nanofluidics research, which mainly concerns the manner of liquid flowing confined in nanosized channels. However, CNT-based NFMs are still far away from practical application because the approaches of preparing them often suffer from several common problems: relatively high cost of CNTs, time consuming and complex process of obtaining high density of vertically-aligned CNTs, and difficulties for achieving large-scale production.[16,21]

Apart from 1D CNTs, the newly emerged 2D graphene, an atomic layer of graphite, also holds outstanding chemical and thermal stabilities, and even superior flexibility and solution processibility.[22,23] More significantly, graphene, especially chemically converted graphene (CCG) or graphene oxide (GO), can form highly ordered films with 2D nanochannels between two graphene sheets by facile filtration-assisted assembly method.[24,25] Recently, a large slip length was also obtained for water in planar confinement between graphene layers by simulations, but results from experiments and the applications in nanofiltration were rarely reported.[26–29] Li and co-workers constructed a kind of wet graphene membrane using wrinkled hydrazine reduced GO, and for the first time investigated its potential application in nanofiltration for nanoparticles and

Y. Han, Z. Xu, Prof. C. Gao
MOE Key Laboratory of Macromolecular Synthesis and Functionalization
Department of Polymer Science and Engineering
Zhejiang University
Hangzhou, 310027, China
E-mail: chaogao@zju.edu.cn

DOI: 10.1002/adfm.201202601

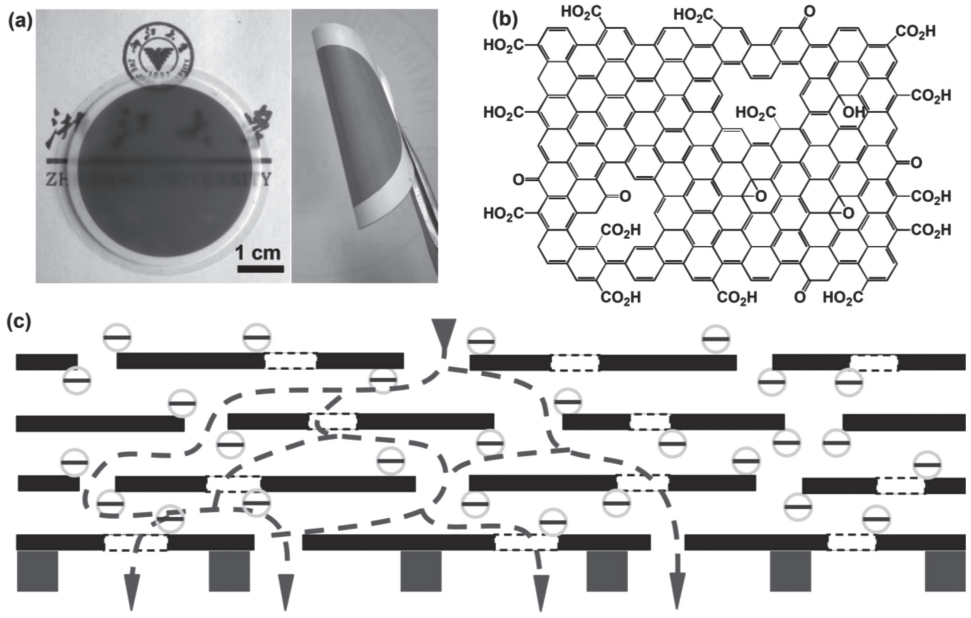

Figure 1. a) Digital photo of an uGNM coated on an AAO disk (left) and a twisted uGNM coated on a PVDF membrane (right). b) Schematic representation of a brGO: graphene sheet with a certain amount of holes and most of the oxidized groups are located on the edges and the periphery of the holes on it. Note that the real graphene sheets extend further than depicted. c) Schematic view for possible permeation route: water molecules go though the nanochannels of the uGNMs and the holes on the graphene sheets and at last reach the pores of supporting membranes. The blank squares present the holes on the graphene sheets (black line). The edges of the brGO and the periphery of the holes are negatively charged.

dyes.[30,31] On the contrary, Geim and co-workers reported that micrometer-thick GO membranes were completely impermeable to liquids, vapors, and gases (even helium), but solely allowed unimpeded evaporation of H_2O; after thermal reduction, the dried graphene membrane became impermeable to any substance including H_2O vapor molecules.[32] This seemingly declares the unavailability of dried graphene films in NFMs.

Here, we designed and fabricated ultrathin (22–53-nm thick) graphene membranes with 2D nanochannels by the simple filtration-assisted assembly strategy, and successfully applied them as NFMs for water purification. Accompanied by the relative high pure water flux (as high as 21.8 L m^{-2} h^{-1} bar^{-1}), the resulting ultrathin graphene nanofiltration membranes (uGNMs) showed high retention rates for organic dyes and moderate retention rates for salts, and the rejection mechanism of separation process for 2D nanochannels was discussed for the first time.

2. Results and Discussion

We designed ultrathin graphene films for possible nanofiltration, because high solvent permeability needs the membrane to be as thin as possible.[5,32] Considering the relative high pressure applied on NFMs (1–20 bar), we used commercialized micro-filtration membranes (e.g., polyvinylidene fluoride (PVDF) or mixed cellulose ester membranes) as supporting substrates. Accordingly, our uGNMs were readily prepared by filtering the extremely dilute base-refluxing reduced GO (brGO) dispersion on such substrate(**Figure 1**a). Generally, CCG is prepared by chemically or thermally reducing GO.[23,25] Herein, we employed Wilson's method to obtain clean brGO by refluxing GO in 0.01 M NaOH aqueous solution for 1 h, since oxidative debris left on GO could be removed by the base washing.[33] The residual functional groups of brGO mostly located at the edges and holes of graphene sheet (Figure 1b).[23,34–36] For a long time, CCG was always controversial for its inherent defects such as holes generated by the oxidation reaction which would blunt the electrical properties and limit the application of CCG in many fields.[35,37] However, for the case of separation membranes, the holes on CCG may be an advantage because more holes mean more permeation "gates" and higher water flux (Figure 1c).

The raw material of brGO was fully characterized by atomic force microscopy (AFM), thermogravimetric analysis (TGA), Raman spectroscopy (Supporting Information Figure S1) and X-ray diffraction (XRD) analysis. After a process of differential centrifugation fractionation, the brGO sheets showed relatively uniform lateral size around 1–2 mm and performed single layered feature deposited on the mica substrates with an average thickness of 0.8 nm (**Figure 2**a,b, and Supporting Information Figure S2). As demonstrated by TGA measurements, GO was greatly reduced into brGO via the base refluxing, as the mass loss before 250 °C declined from 36.5% of GO to 11.7% of brGO (Figure 2c). Two main peaks at 2q = 12.6° and 24.1° are observed in the XRD pattern of brGO in powder state (Figure 2d), corresponding to interlayer spacing of ≈0.7 and 0.4 nm, respectively. The double peaks in XRD indicated a certain amount of functional groups still left on brGO, endowing single-layer dispersibility of brGO in water.[38] This fine dispersibility is crucial for achieving well-packed layer-structured film. Notably, the uGNMs were so thin that the X-ray diffraction

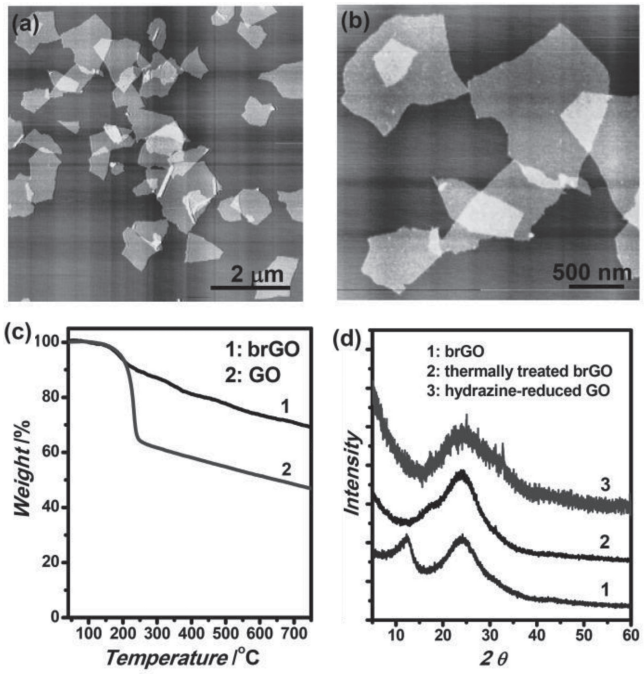

Figure 2. a,b) AFM images of brGO sheets dispersed on a mica. c) Thermogravimetric analysis in nitrogen of GO and brGO. d) XRD patterns of base-refluxing reduced GO (or brGO), hydrazine-reduced GO, and thermally treated brGO at 220 °C in vacuum.

signal is too weak to detect. As a result, in this case the XRD data can only demonstrate the reduction of GO but gave limited information about the interlayer spacing of the uGNMs. In fact, the interlayer spacing of the uGNMs was tunable by the degree of hydration and could be more than 1 nm after full hydration.[39] In addition, the average water contact angle increased from 43° on GO film to 70° on the uGNM (Supporting Information Figure S3), indicating the more hydrophobic nature of brGO.

In order to understand the manner in which graphene sheets stacked on the supporting micro-pours filters, a sample filtrated on a smooth and rigid anodic aluminum oxide (AAO) membrane was characterized by transmission electron microscopy (TEM) and scanning electron microscopy (SEM) (**Figure 3** and Supporting Information Figure S4). Graphene sheets assembled on the substrate forming a well-packed laminated ultrathin film. The surface of the membrane is smooth and no obvious corrugation was observed except for some ripples formed by the edges of brGO sheets. This compact structure of our uGNMs is essentially different from that of previously reported wet graphene papers, in which corrugations of graphene sheets acted as the water channels.[30] In order to obtain the uniform, smooth and tightly stacked membranes, extremely dilute brGO dispersions (as low as 0.36 mg mL^{-1}) were applied in our experiments. Besides, relatively long filtration time (≈3 h) and a drying process in vacuum were also necessary. In our uGNMs, smoothness and flattening are quite important to form uniform 2D nanochannels for water transport and to achieve high retention performance.[12] The average thickness of graphene layer with the most loading brGO (34 mg m^{-2}) was measured to be 53 nm by AFM (Figure 3e and Supporting Information Figure S5), and others with less brGO loadings were estimated as 22, 26, 33, and 44 nm assuming that the thickness is proportional to the loading (**Table 1**). The thickness determined from SEM (Figure 3c) was ≈40 nm, in reasonable agreement with AFM (Figure 3e).

The thickest uGNM is so thin that it is still transparent on an anodic aluminum oxide (AAO) disk, and we can easily distinguish the characters behind it by naked eyes (Figure 1a), and the sub-micrometer pores of AAO covered by uGNM can be even seen under SEM (Figure 3b). Moreover, the uGNMs are thin enough to have excellent flexibility and it can be bent randomly without breakage (Figure 1a), providing a flexible basis for packaging uGNMs into more complex membrane modules which is still an unsolved challenge for carbon-based membranes.[40] Notably, although the graphene membranes on the microporous substrates are only tens of nanometers in thickness, they are stable in water for least half a year without any visible change in appearance, because most of the oxygen-contained

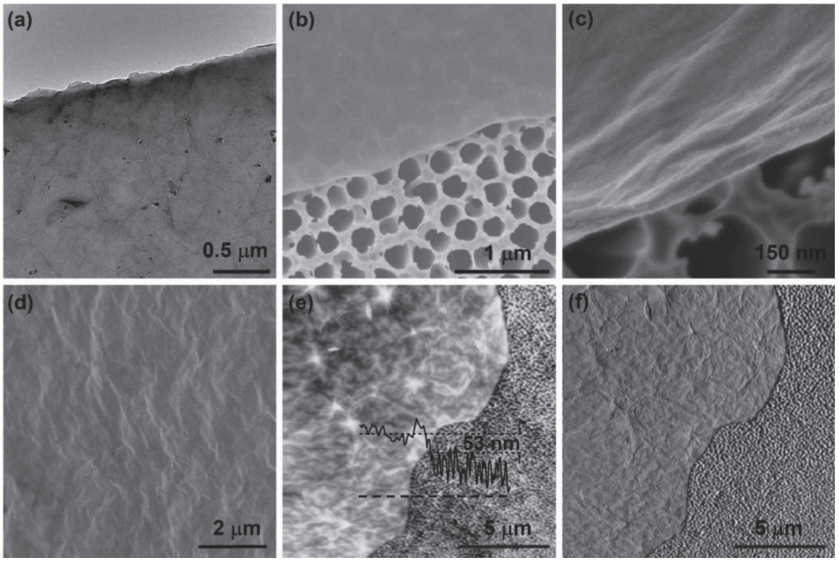

Figure 3. a) TEM image of a free standing ultrathin graphene membrane on a copper mesh. The edges of the graphene sheets could be distinguished clearly from the dark lines in the image. b) SEM image (top view) of the coating of an uGNM on an AAO disk. The top half of the image shows the uniform and smooth coating of brGO sheets, whereas the bottom half shows the porous structure of the bare AAO disk. c) Amplified SEM image (top view) of the coating of an uGNM on an AAO disk with more details about the surface morphology and the cross-section. The top half of the image shows the coating of brGO sheets, whereas the bottom half shows the bare AAO disk. d) SEM image (top view) of the surface morphology of an uGNM deposited on a mixed cellulose ester membrane with pore size of 0.22 mm, indicating the relatively smooth surface of the uGNM. The loading of all these uGNMs was 34 mg m^{-2}. e) AFM height and f) phase images of an uGNM coated on an AAO disk (pore size 200 nm). The right part of the image shows the bare AAO support, while the remaining parts shows the surface morphology of the uGNM.

Table 1. Retention of organic dyes for uGNMs with different brGO loadings and brGO layer thickness.

brGO loading [mg m^{-2}]	Thickness [nm]	Pure water flux J_0 [L m^{-2} h^{-1} bar^{-1}]	MB[a]			DR 81[a]		
			Retention [%]	J/J_0 [%][b]	C/C_0[c]	Retention [%]	J/J_0 [%][b]	C/C_0[c]
14.1[d]	22	21.81	99.2	90.0	1.27	99.9	89.6	1.31
17.0[e]	26	12.62	99.7	91.1	1.30	99.8	89.7	1.33
21.2[e]	33	5.00	99.7	89.4	1.32	99.9	87.2	1.33
28.3[e]	44	4.37	99.6	90.4	1.33	99.9	95.8	1.34
34.0[e]	53	3.26	99.8	95.0	1.36	99.9	95.6	1.35

[a]The concentration of feed dye solution C_0 was 0.02 mM. [b]The ratio of permeate flux of the dye solution J to the pure water flux J_0. [c]Concentration ratio of upper stream (C) when the permeation volume was 10 mL to the original feeding solution (C_0, 35 mL). [d]The applied pressure was 1 bar. [e]The applied pressure was 5 bar.

groups on GO were removed during the base refluxing. Such robust nature is critical to water purification membranes.

We tested pure water fluxes to evaluate the performance of uGNMs. A series of uGNMs were fabricated for water transporting with different loadings of brGO, ranging from 14.1 to 34.0 mg m^{-2} (Table 1). The fluxes were recorded until steady state was reached, typically after half an hour. The initial flux could be as large as 51 L m^{-2} h^{-1} bar^{-1} for our uGNMs (Supporting Information Figure S6), while at steady-state the value dropped to ≈1/2 of the initial flux (21.8 L m^{-2} h^{-1} bar^{-1}). As shown in **Figure 4**a, under a low pressure of 1 bar, an exponential decrease in the water flux was observed with increasing brGO loading. At a constant brGO loading, the water permeation rate increased linearly with increasing applied pressure (Figure 4b). A maximum pressure of 7 bar was applied due to the limitation of our filtration device, but it is believed that these membranes could withstand higher pressures due to the outstanding mechanical properties of graphene and the supporting effect of the substrates. As presented in Figure 4a, the uGNM with the lowest loading of brGO (14.1 mg m^{-2}) showed the highest water flux under a steady state (21.8 L m^{-2} h^{-1} bar^{-1}), which was a considerable high value compared with the commercial NFMs (for example, the pure water flux of commercial low desalting membrane UTC60 is 15.4 L m^{-2} h^{-1} bar^{-1}).[1] This value is also comparable with that of vertically-aligned CNTs membranes reported recently (72 L m^{-2} h^{-1} bar^{-1}).[41]

Theoretically, the Hagen–Poiseuille equation was usually employed to estimate the mass flow through porous materials per unit area when the fluid behaves as a classical liquid.[14,32,41] Given the average size of water nanochannels of uGNMs, under the pressure of ΔP (1 bar), the Hagen–Poiseuille equation can be transformed into following form:

$$Flux \approx \frac{h^4 \cdot \Delta P}{12L^2 \cdot \eta \cdot \Delta x} \quad (1)$$

where h is the vertical space between adjacent graphene sheets, L the average lateral length of the brGO sheets (1 μm in our case), η the viscosity of water (0.001 Pa s at 20 °C), and Δx the thickness of uGNM. In our case, we assumed the Hagen–Poiseuille equation for flow through thin parallel plates was $Q = (h^3 L \Delta p)/(12 \eta l)$, the effective channel length was $l = L \Delta x/h$, and an areal density was $1/L^2$. For the thickest uGNM ($\Delta x \approx 53$ nm), this equation yields a flux of 1.4×10^{-4} L m^{-2} h^{-1} bar^{-1}, four orders of magnitude smaller than our experimental value (3.3 L m^{-2} h^{-1} bar^{-1}). One possible explanation is that water molecules might go through the defects of graphene sheets (Figure 1c), leading to smaller L and higher flux calculated from Equation (1).

Another possible explanation for such high flux could be the slip flow theory. The basic assumptions of Hagen–Poiseuille equation are laminar flow and no-slip (or liquid flow with zero velocity) at the boundary layer, and the departure of experimental flux from the classical equation suggests that the velocity of the liquid flow at graphene wall is not zero. Similarly, in the cases of CNTs with a diameter smaller than 10 nm, a flow enhancement of 10^3–10^4 fold was also found for water confined in 1D nanochannels.[14,41] Such a fast transport of water though small-diameter CNTs was mainly ascribed to the two reasons of (1) low friction between water and hydrophobic carbon wall and (2) ordered hydrogen bonds formed by the single file of water molecules.[9–11,14] Likewise, our uGNMs also possess frictionless carbon walls and nanocapillaries that are in 2D form (Figure 1c). Notably, the oxygen-contained groups on graphene sheets would block water molecules because of the strong interaction between them. Thus only the graphene regions without functional groups were responsible for the fast transport of water.[32] This explanation was supported by the fact that the neat GO membrane showed only half of pure water flux of brGO membranes at the same conditions. Furthermore, we measured the flux of a number of liquids with different polarities, such as isopropanol, ethanol, hexane, cyclohexane, and toluene. According to the slip flow theory, more hydrophobic liquid would lead to lower flux under the same pressure, because of greater interaction between more hydrophobic liquid and graphene walls. As shown in Figure 4c, the most hydrophilic liquid of water showed the highest flux, and the most hydrophobic liquid of hexane showed the lowest flux. As expected by the slip flow theory, the fluxes decreased with the decreasing of polarities, which is in agreement with the case of CNTs.[9,11,14] According to Equation (1), flux is in inverse proportion to liquid viscosity (η). But in fact, as shown in Figure 4c, the flux of hexane with small viscosity (η = 0.33 mPa s at 20 °C) is much lower than that of water with relatively high viscosity (η = 1 mPa s at 20 °C), which implies that the real flux of the thicker uGNMs can not be fully described

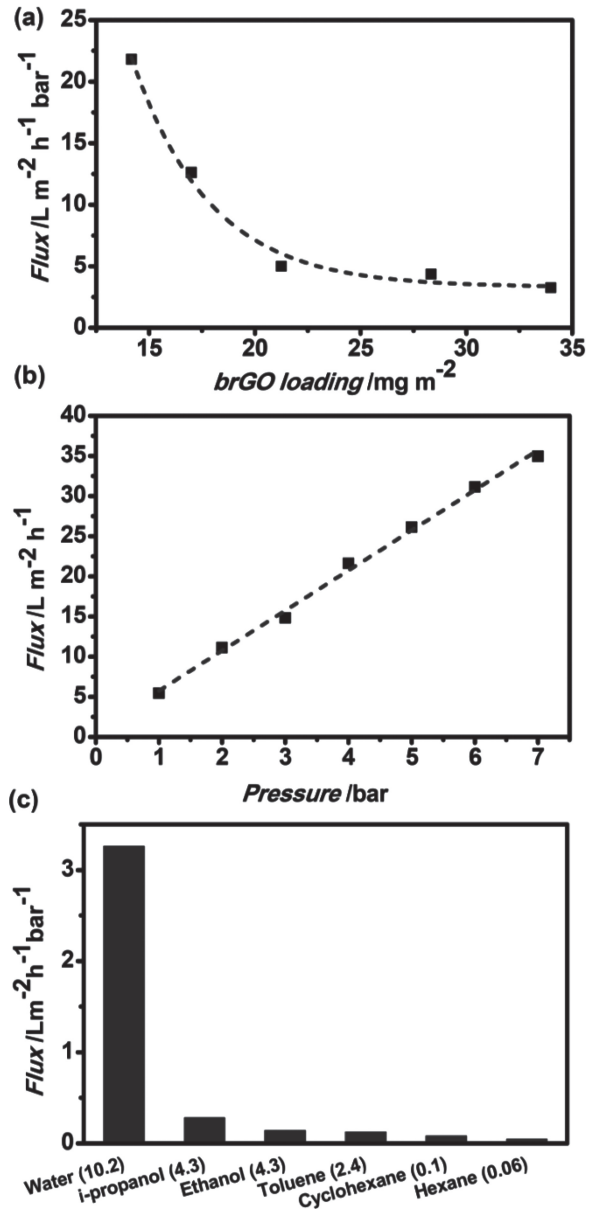

Figure 4. a) Variations of pure water flux as a function of brGO loading coated on the membranes. The pressure applied here was 1 bar. b) Water flux versus pressure applied on the uGNM with a brGO loading of 28.3 mg m^{-2}. c) Flux for various liquids as a function of their polarities under a pressure of 5 bar. The polarities were listed in the parenthesis behind each the name of the liquids. The uGNM used here had a brGO loading of 34.0 mg m^{-2}.

by Equation (1). Actually, slip flow theory itself is still a controversial topic for lack of enough direct proof, more experiments should be carried out to get deeper understanding for the liquid transport in 2D nanochannels.

Subsequently, we further investigated the nanofiltration performance of uGNMs for organic dyes. Retention measurements with dye solutions of methyl blue (MB) and direct red 81 (DR 81) were carried out using pressure driven filtration at relatively low pressure (no more than 5 bar), followed by UV-vis analysis of the dye concentrations of permeate and feed solutions. The results are listed in Table 1. The retention increased with increasing the thickness of brGO layer of uGNMs. For the 53 nm uGNM, the retentions for MB and DR 81 are as high as 99.8% and 99.9%, respectively. As shown in Table 1, the flux went down a little when filtrating dye solution but still maintaining nearly 90% of the pure water flux. According to the structure of uGNMs, the retention mechanism could be possibly attributed to three main models: (1) direct absorption of dye molecules by brGO, (2), physical sieving by 2D nanochannels which is controlled by channel sizes, and (3) electrostatic interaction between charged dyes and the negatively charged groups of brGO.[1,3,42] Previous reports showed that graphene contained filters could decolor aqueous solutions by adsorption of dyes.[43] In fact, the extent of dye absorption into the membrane could be probed by measuring the concentration change of the upper stream. If the filtration process is dominated by absorption, the concentration of the upper stream would not change obviously with increasing permeation volume. In Table 1 we listed the concentration ratio of upper stream (C) when the permeation volume was 10 mL to the original feeding solution (35 mL, C_0). The ideal value of C/C_0 is 1.4 if there is no dye absorption into the membrane at all and the rejection rate is 100%. The experimental values are 1.27–1.36, and the thicker uGNMs showed higher values of C/C_0, indicating less dyes absorption. For the 44 nm uGNM, the dye concentration (DR 81) in upper stream increased gradually when the permeation volume was 5, 10 and 15 mL under a pressure of 5 bar (**Figure 5**), and the dark red DR 81 solution had also turned into colorless after filtration (see the inset in Figure 5). Our result indicates that the dye separation of our uGNMs is not dominated by the absorption mechanism. Because the average size of the 2D nanocapillaries of uGNMs is smaller than that of dye molecules (MB 20 Å, DR 81 22.8 Å, estimated using a Molecular Mechanics 2 method in Chem3D), physical sieving by nanochannels of the uGNMs is believed as the dominant factor in retention of organic molecules. However, the effect of electrostatic interaction between charged dyes and the negatively

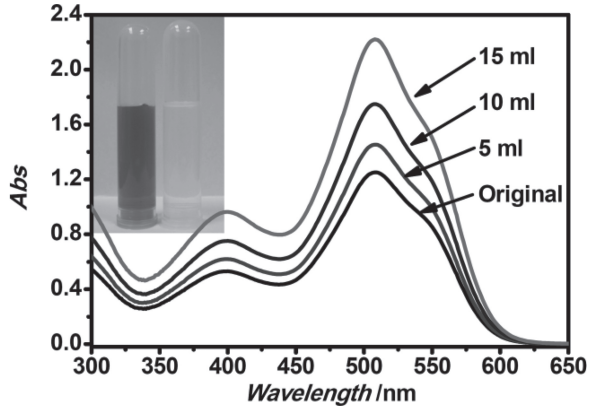

Figure 5. UV-vis absorbance changes of upper stream of DR 81 solution when the permeation volume was 5, 10, and 15 mL under the pressure of 5 bar. Inset: the photographic image showed the color change of 0.02 mM DR 81 solution (left) and the collected filtrate (right). The uGNM used here had a brGO loading of 28.3 mg m^{-2}.

charged groups of brGO could not be ignored. To understand this, we have to recall the structure of uGNMs (Figure 1b), which is negatively charged because of the carboxylic groups on brGO (the zeta potential of brGO is –43 mV at 25 °C).[34,36] Considering that MB and DR is negatively charged, the electrostatic repulsion could also play an important role in rejecting negatively charged dye molecules. To prove the important role of electrostatic interaction in retention mechanism, we tested the retention of 33 nm uGNM to electroneutral rhodamine B (RB). The retention for RB was found to be 78%, much lower than that for MB and DR 81, confirming the importance of electrostatic repulsion for separating charged dyes. Given that different reducing methods may result in distinct CCG sheets with different degrees of functionalization, and their corresponding membranes possibly have variant filtration performances, we also designed and fabricated ultrathin membranes made of hydrazine-reduced (hGM) and thermally reduced GO (tGM). The corresponding XRD data were shown in Figure 2d. The hGM showed much lower retention for RB (40%) than uGNM (78%) with similar water flux. The higher retention of uGNMs possibly resulted from more uniform and smaller nanochannels formed by base-refluxed GO, since hydrazine-reduced GO possessed much more wrinkles and corrugations (Supporting Information Figure S7).[30] Interestingly, after thermal treatment of uGNM at 220 °C for 1 h, the resulting tGM exhibited only half of pure water flux while remained similar retention of RB (76%) to original uGNMs. This result could be explained by the decrease of nanochannels size (or d space between adjacent brGO sheets) after thermal treatment, since only one peak at $2\theta = 24.3°$ was detected in XRD measurement (Figure 2d). It seems our result is not well coincident with Geim's report in which the thermally reduced GO membrane became 100 times less permeable to water. The difference could be contributed to two main reasons. Firstly, Geim's membranes were 1–2 orders of magnitude thicker than our uGNMs, and thicker membranes means more blocks for water transport. Secondly, in our experiments, uGNMs fully contacted with bulk water, and this high humidity could broaden the graphene capillary as demonstrated in some early reports, facilitating the water transport.[32,44] Apparently, different type of reducing treatment leads to different type, location and degree of remaining functional groups on graphene sheets. The residual functional groups play an important role in determining the morphology of graphene and the interspace between graphene sheets. As a result, the performance of graphene filtration membrane largely depends on the reducing method. The low dye retentions at low brGO loadings suggests the thinner uGNMs may act as a kind of conventional porous NFMs. Judging from the rejection performance, the pore size of the thinnest uGNM seems to be ≈1–2 nm. The porosity (ε) of the thinnest uGNM is ≈0.68% as calculated from the Hagen–Poiseuille equation ($\varepsilon = 8\ Flux \cdot \eta \cdot \Delta x / (r^2 \cdot \Delta p)$, where r is the radius of pores).

NFMs are also usually applied to separate ions from water, although the retention is moderate compared with reverse osmosis membranes.[2,45] Additionally, the retention performance of salts can reflect the charge characteristics of membranes. Thus, as an exploratory study, we tested the retentions of our uGNMs to four kinds of salt NaCl, Na_2SO_4, $MgCl_2$ and $MgSO_4$ at the concentration of 0.02 M under a pressure of 5 bar. A high rejection of Na_2SO_4 was achieved at ≈60%. As shown in **Figure 6**, the retention (R) sequence of the salt solutions was R (Na_2SO_4) > R (NaCl) > R ($MgSO_4$) > R ($MgCl_2$). This sequence can be explained by Donnan exclusion theory that is usually used to explain the retention mechanism for charged NFMs.[2,17,45] As mentioned above, uGNMs are negatively charged because of the carboxylic groups at edges and holes of brGO sheets. According to the Donnan exclusion theory, the Donnan potential at the interphase of solution and membrane tends to exclude co-ions from the membrane. In order to keep the electroneutrality of the solution on each side of the membrane, the counter ions have to be rejected as well. As a result, the retention of salt is sensitive to the valences of the cationic (Z+) and anionic (Z–) species of the salts. Donnan theory provides the following equation for the retentions of salts,

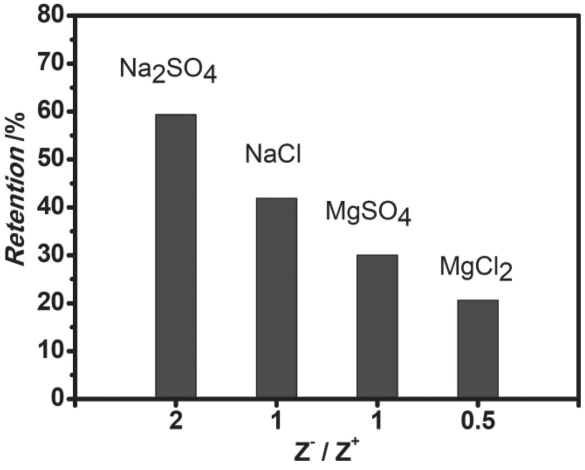

Figure 6. Retention measured for four different salt solutions (0.02 M) with different ion valences. The uGNM used here had a brGO loading of 34.0 mg m^{-2}, and a pressure of 5 bar was applied.

$$R = 1 - \frac{C_B^m}{C_B} = 1 - \left(\frac{|Z_B|\, C_B}{|Z_B|\, C_B^m + C_X^m} \right)^{|Z_B|/|Z_A|} \quad (2)$$

where Z_B and Z_A are the valence of the co-ions and counterions, C_B and $C_B{}^m$ the concentrations of the co-ions in solution and membrane phase, and $C_X{}^m$ is the membrane charge concentration. From this equation, it can be qualitatively calculated that the retention sequence of the salts used in our experiments is R (Na_2SO_4) > R (NaCl) ≈ R ($MgSO_4$) > R ($MgCl_2$).[2] Our experimental sequence is identical with the calculated one, revealing that the salt rejection of the uGNMs is mainly determined by the Donnan exclusion. It should be noted that, the salts retentions for uGNMs are higher than and comparable to the CNTs-based NFMs at the concentration of 20 mM made by Bakajin and co-workers,[17] but lower than some of commercial desalination NFMs. Two main reasons might contribute to the low salt retention. Firstly, the operation pressure in our cases is quite low (<8 bar) owing to the limitation of our filtration device. Many studies demonstrated that retention of salts decreases with a decrease in applied pressure.[1,46] Secondly, there might be some pores larger than 2 nm and even unzipped slits in the CCG sheets of uGNMs caused by the strong oxidation,

lowering the salt retention. Hence, further optimization in both aspects of filtration device and graphene membranes is needed in future studies. As demonstrated above, uGNMs showed high retention for organic dyes and moderate retention for salts, indicating their potential application in the concentration and separation of dyes.

3. Conclusions

In summary, dried, ultrathin, and robust graphene nanofiltration membranes were firstly fabricated from brGO by vacuum-assisted assembly strategy. The brGO sheets stacked with each other forming sub-1-nm sized 2D nanocapillaries, and the hydrophobic carbon nanochannels favor high water flux. The uGNMs showed excellent performance for retention of organic dyes, especially for the charged dyes, based on the mechanism of physical sieving and electrostatic interaction. The Donnan exclusion dominated the salt rejection of the graphene membranes. The uGNMs are extremely thin, and less than 35 mg of brGO is needed for making a square meter membrane. Compared with the membranes made of aligned CNTs, the stacked graphene membranes have the advantages of low cost and simple fabrication process. The uGNMs perfectly integrated the merits of both graphene (such as highly thermal stability, fine chemical resistance, and excellent mechanical property) and polymer materials (such as high flexibility, simple solution-based processibility, and scalability), opening a door for the next generation of NFMs. Further improvement of uGNMs might include optimizing the size and density of holes on the graphene sheets, adjusting the space between graphene sheets, and increasing the antifouling property by chemical modification.

4. Experimental Section

Materials: Graphite powder (40 μm) was purchased from Qingdao Henglide Graphite Co., Ltd. All the other reagents were purchased from Aldrich and used as received.

Characterization: UV-vis spectra were obtained on a Varian Cary 100 Bio UV-vis spectrophotometer. AFM images were obtained on a NSK SPI3800, under tapping mode. TEM studies were conducted on a JEOL JEM2010 electron microscope at 200 kV. TGA was carried out on a Perkin-Elmer Pyris 6 TGA instrument under nitrogen with a heating rate of 10 °C min^{-1}. Raman measurements were conducted on a LabRam-1B Raman spectroscope equipped with a 514 nm laser source. The contact angle measurements were carried out on a DropMeter A-200 (MAIST Vision Inspection & Measurement Ltd. Co.). SEM images were obtained by Hitachi S4800 field-emission SEM system. XRD was carried out on X' Pert PRO diffractometer equipped with Cu Ka radiation (40 kV, 40 mA). Zeta potentials were measured by laser Doppler electrophoresis using a Zeta-Nanosizer (Nano ZS, Malvern Instruments Ltd., Worcestershire, UK).

Preparation of Narrow-Dispersed GO and Base-Refluxing Reduced GO (brGO): Firstly, a modified Hummers' method was applied to prepare GO which was described in previous studies.[47–50] The resulting GO aqueous dispersion (1 mg mL^{-1}) was sonicated for 10 min followed by centrifugation at 10 000 rpm for 15 min. The supernatant was collected and the sediment was re-dispersed in de-ionized water. Repeat the centrifugation procedure four times and collect all the supernatant to obtain the centrifugal classified and narrow-dispersed GO dispersion.[51]

The as-prepared centrifugal classified GO aqueous dispersion (50 mL, 0.5 mg mL^{-1}) and NaOH (20 mg) were added into 100 mL Schlenk flask with stirring under nitrogen flow. After stirring for 0.5 h, the system was heated to reflux for an hour, resulting in uniform dark black dispersion. After cooling down to room temperature, the dispersion was centrifuged at 17 900 rpm for an hour. Discard the light dark supernatant and wash the sediment three times by deionized water, giving the stable brGO.[33]

Fabrication of uGNMs: Extremely dilute brGO dispersion was prepared by adding a certain amount of brGO into water (50 mL) followed by 10 min ultrasonication. In order to fabricate uGNMs with different thickness, a series of dilute brGO dispersion were prepared with concentrations ranged from 0.36 to 0.864 μg mL^{-1}. Then the dilute brGO dispersion (50 mL) was filtrated under vacuum on microfiltration membranes such as mixed cellulose ester membranes, PVDF membranes, or AAO membranes (Anodisc 47 purchased from Whatman) with pore size of around 200 nm. The uGNM system composed of ultrathin graphene layer and the substrate membrane (note: we use only uGNMs to represent the composite membrane in the paper) was dried in vacuum for 24 h at 40 °C before use. Samples for AFM and SEM characterizations were prepared by stripping part of the graphene layer coated on an AAO disk by tape. The sample for TEM characterization was prepared by the following two steps: (1) to exfoliate the neat graphene membrane from the composite membrane by immersing the composite membrane with an AAO substrate in water, (2) to transport a piece of free standing graphene layer onto a TEM copper mesh and put it in vacuum oven overnight at 40 °C before characterization.

As control experiments, we also prepared graphene membranes made of hydrazine-reduced GO by the same protocol mentioned above (experiment details of preparing hydrazine-reduced GO are given in the Supporting Information).[25,30] Moreover, some uGNMs were heated at 220 °C in a vacuum for further investigation.[32] Herein, the hydrazine-reduced ultrathin graphene membrane is designated as hGM, and the thermally treated graphene membrane is denoted as tGM.

Measurements of Pure Water Flux and Retention: The pure water flux and retention measurements were performed on a dead end filtration device driven by nitrogen gas as shown in Supporting Information Figure S8. The area for water permeation in this device is 2.83 cm^2. The selected uGNM was fixed at the bottom of the water tanker. The applied pressure could be adjusted from 0 to 7 bar. Pure water flux was obtained by measuring the mass of water collected every two minutes under a certain pressure. As shown in Supporting Information Figure S6, for a typical flux measurement, pure water flux decayed with time rapidly at first, and was steady after about half an hour, and the steady-state value was recorded as the flux of the uGNMs. Similar declines for CNTs membranes were also reported in Hinds' work, where initial water flux was preferred.[14] In our cases, the initial water flux could be as large as 51 L m^{-2} h^{-1} bar^{-1}.

Supporting Information

Supporting Information is available from the Wiley Online Library or from the author.

Acknowledgements

Financial support from the National Natural Science Foundation of China (No. 51173162 and No. 20974093), Qianjiang Talent Foundation of Zhejiang Province (2010R10021), the Fundamental Research Funds for the Central Universities (2011QNA4029), Research Fund for the Doctoral Program of Higher Education of China (20100101110049), and Zhejiang Provincial Natural Science Foundation of China (No. R4110175) are kindly acknowledged. The authors are grateful to Prof. Zhikang Xu, Dr. Linshu Wan, and Dr. Lin Zhang for helpful discussions. They also thank Prof. Baoku Zhu and Mr. Zhikan Yao for their help in the filtration experiments.

Received: September 9, 2012
Revised: December 13, 2012
Published online: February 26, 2013

[1] K. O. Agenson, J. I. Oh, T. Urase, *J. Membr. Sci.* **2003**, *225*, 91.
[2] J. Schaep, B. Van der Bruggen, C. Vandecasteele, D. Wilms, *Sep. Purif. Technol.* **1998**, *14*, 155.
[3] K. Kimura, G. Amy, J. E. Drewes, T. Heberer, T. U. Kim, Y. Watanabe, *J. Membr. Sci.* **2003**, *227*, 113.
[4] B. Van der Bruggen, M. Manttari, M. Nystrom, *Sep. Purif. Technol.* **2008**, *63*, 251.
[5] S. Karan, S. Samitsu, X. Peng, K. Kurashima, I. Ichinose, *Science* **2012**, *335*, 444.
[6] L. Cot, A. Ayral, J. Durand, C. Guizard, N. Hovnanian, A. Julbe, A. Larbot, *Solid State Sci.* **2000**, *2*, 313.
[7] S. Benfer, P. Arki, G. Tomandl, *Adv. Eng. Mater.* **2004**, *6*, 495.
[8] L. F. Dumée, K. Sears, J. Schütz, N. Finn, C. Huynh, S. Hawkins, M. Duke, S. Gray, *J. Membr. Sci.* **2010**, *351*, 36.
[9] M. Majumder, N. Chopra, R. Andrews, B. J. Hinds, *Nature* **2005**, *438*, 44.
[10] A. Kalra, S. Garde, G. Hummer, *Proc. Natl. Acad. Sci. USA* **2003**, *100*, 10175.
[11] G. Hummer, J. C. Rasaiah, J. P. Noworyta, *Nature* **2001**, *414*, 188.
[12] K. Falk, F. Sedlmeier, L. Joly, R. R. Netz, L. Bocquet, *Nano Lett.* **2010**, *10*, 4067.
[13] R. Wan, H. Lu, J. Li, J. Bao, J. Hu, H. Fang, *Phys. Chem. Chem. Phys.* **2009**, *11*, 9898.
[14] M. Majumder, N. Chopra, B. J. Hinds, *ACS Nano* **2011**, *5*, 3867.
[15] B. J. Hinds, N. Chopra, T. Rantell, R. Andrews, V. Gavalas, L. G. Bachas, *Science* **2004**, *303*, 62.
[16] M. Yu, H. H. Funke, J. L. Falconer, R. D. Noble, *Nano Lett.* **2009**, *9*, 225.
[17] F. Fornasiero, H. G. Park, J. K. Holt, M. Stadermann, C. P. Grigoropoulos, A. Noy, O. Bakajin, *Proc. Natl. Acad. Sci. USA* **2008**, *105*, 17250.
[18] S. T. Mostafavi, M. R. Mehrnia, A. M. Rashidi, *Desalination* **2009**, *238*, 271.
[19] J. Wu, K. S. Paudel, C. Strasinger, D. Hammell, A. L. Stinchcomb, B. J. Hinds, *Proc. Natl. Acad. Sci. USA* **2010**, *107*, 11698.
[20] K. Sears, L. Dumee, J. Schuetz, M. She, C. Huynh, S. Hawkins, M. Duke, S. Gray, *Materials* **2010**, *3*, 127.
[21] S. Kim, J. R. Jinschek, H. Chen, D. S. Sholl, E. Marand, *Nano Lett.* **2007**, *7*, 2806.
[22] A. K. Geim, K. S. Novoselov, *Nat. Mater.* **2007**, *6*, 183.
[23] D. R. Dreyer, S. Park, C. W. Bielawski, R. S. Ruoff, *Chem. Soc. Rev.* **2010**, *39*, 228.
[24] D. A. Dikin, S. Stankovich, E. J. Zimney, R. D. Piner, G. H. B. Dommett, G. Evmenenko, S. T. Nguyen, R. S. Ruoff, *Nature* **2007**, *448*, 457.
[25] D. Li, M. B. Müller, S. Gilje, R. B. Kaner, G. G. Wallace, *Nat. Nanotechnol.* **2008**, *3*, 101.
[26] A. Maali, T. Cohen-Bouhacina, H. Kellay, *Appl. Phys. Lett.* **2008**, *92*, 053101.
[27] S. K. Kannam, B. D. Todd, J. S. Hansen, P. J. Daivis, *J. Chem. Phys.* **2012**, *136*, 024705.
[28] G. Cicero, J. C. Grossman, E. Schwegler, F. Gygi, G. Galli, *J. Am. Chem. Soc.* **2008**, *130*, 1871.
[29] W. Xiong, J. Z. Liu, M. Ma, Z. Xu, J. Sheridan, Q. Zheng, *Phys. Rev. E* **2011**, *84*, 056329.
[30] L. Qiu, X. H. Zhang, W. R. Yang, Y. F. Wang, G. P. Simon, D. Li, *Chem. Commun.* **2011**, *47*, 5810.
[31] X. Yang, L. Qiu, C. Cheng, Y. Wu, Z. F. Ma, D. Li, *Angew. Chem., Int. Ed.* **2011**, *50*, 7325.
[32] R. R. Nair, H. A. Wu, P. N. Jayaram, I. V. Grigorieva, A. K. Geim, *Science* **2012**, *335*, 442.
[33] J. P. Rourke, P. A. Pandey, J. J. Moore, M. Bates, I. A. Kinloch, R. J. Young, N. R. Wilson, *Angew. Chem., Int. Ed.* **2011**, *50*, 3173.
[34] J. T. Paci, T. Belytschko, G. C. Schatz, *J. Phys. Chem. C* **2007**, *111*, 18099.
[35] K. Erickson, R. Erni, Z. Lee, N. Alem, W. Gannett, A. Zettl, *Adv. Mater.* **2010**, *22*, 4467.
[36] C. Mattevi, G. Eda, S. Agnoli, S. Miller, K. A. Mkhoyan, O. Celik, D. Mostrogiovanni, G. Granozzi, E. Garfunkel, M. Chhowalla, *Adv. Funct. Mater.* **2009**, *19*, 2577.
[37] C. Gómez-Navarro, J. C. Meyer, R. S. Sundaram, A. Chuvilin, S. Kurasch, M. Burghard, K. Kern, U. Kaiser, *Nano Lett.* **2010**, *10*, 1144.
[38] H. K. Jeong, Y. P. Lee, M. H. Jin, E. S. Kim, J. J. Bae, Y. H. Lee, *Chem. Phys. Lett.* **2009**, *470*, 255.
[39] K. Raidongia, J. Huang, *J. Am. Chem. Soc.* **2012**, *134*, 16528.
[40] D. R. Paul, *Science* **2012**, *335*, 413.
[41] J. K. Holt, H. G. Park, Y. M. Wang, M. Stadermann, A. B. Artyukhin, C. P. Grigoropoulos, A. Noy, O. Bakajin, *Science* **2006**, *312*, 1034.
[42] L. D. Nghiem, A. I. Schafer, M. Elimelech, *Sep. Sci. Technol.* **2005**, *40*, 2633.
[43] W. Gao, M. Majumder, L. B. Alemany, T. N. Narayanan, M. A. Ibarra, B. K. Pradhan, P. M. Ajayan, *ACS Appl. Mater. Interfaces* **2011**, *3*, 1821.
[44] A. Lerf, A. Buchsteiner, J. Pieper, S. Schottl, I. Dekany, T. Szabo, H. P. Boehm, *J. Phys. Chem. Solids* **2006**, *67*, 1106.
[45] J. M. M. Peeters, J. P. Boom, M. H. V. Mulder, H. Strathmann, *J. Membr. Sci* **1998**, *145*, 199.
[46] W. R. Bowen, J. S. Welfoot, *Chem. Eng. Sci.* **2002**, *57*, 1121.
[47] H. K. He, C. Gao, *Chem. Mater.* **2010**, *22*, 5054.
[48] Z. Xu, C. Gao, *Macromolecules* **2010**, *43*, 6716.
[49] Z. Xu, C. Gao, *ACS Nano* **2011**, *5*, 2908.
[50] Z. Xu, Y. Zhang, P. Li, C. Gao, *ACS Nano* **2012**, *6*, 7103.
[51] Z. Xu, C. Gao, *Nat. Commun.* **2011**, *2*, 571.